European Review for Medical and Pharmacological Sciences 2020; 24: 3254-3266

Imaging of the muscle and bone from benchtop to bedside

H.-M. WANG[1], A. KHORADMEHR[2], A. TAMADON[2], E. VELEZ[3], I. NABIPOUR[4], N. JOKAR[5], M. ASSADI[5], A. GHOLAMREZANEZHAD[3]

[1]Department of Integrative Medicine and Neurobiology, School of Basic Medical Sciences; Institute of Acupuncture and Moxibustion, Fudan Institutes of Integrative Medicine, Fudan University, Shanghai, China
[2]The Persian Gulf Marine Biotechnology Research Center, The Persian Gulf Biomedical Sciences Research Institute, Bushehr University of Medical Sciences, Bushehr, Iran
[3]Department of Diagnostic Radiology, Keck School of Medicine, University of Southern California (USC), Los Angeles, CA, USA
[4]The Persian Gulf Tropical Medicine Research Center, [5]The Persian Gulf Nuclear Medicine Research Center; The Persian Gulf Biomedical Sciences Research Institute, Bushehr University of Medical Sciences, Bushehr, Iran

Huimei Wang and Arezoo Khoradmehr contributed equally to this work

Abstract. – Studies have begun to show that muscles and bones play a role in the regulation of biological functions through a combination of biomechanical and biochemical signals. *In vivo* and *ex vivo* imaging techniques are crucial in the understanding of the morphology and architecture of muscle and bone for further understanding of musculoskeletal physiology and pathophysiology. This systematic review of the literature summarizes current knowledge and outlines new insights into the functions of muscle and bone elucidated by imaging techniques, with a focus on the recent advances in the musculoskeletal system enabled by novel technologies, such as CLARITY, Fast Free-of-Acrylamide Clearing Tissue (FACT), computed tomography (CT), and positron emission tomography (PET). This may serve as guidance for the development of new strategies to prevent and diagnose motor or metabolism disorders related to the malfunction of muscle and bone.

Key Words:
Imaging, Muscle, Bone, Biomechanics, Basic research.

Introduction

The impairment of muscle and bone function can be caused by a wide array of pathologies. These malfunctions can lead to extreme fatigue, pain, and issues with mobility, greatly impairing the quality of life[1-3]. Imaging is an essential part of the diagnosis and management of the majority of muscle and bone-related diseases; however, it remains to be determined which is the optimal imaging method for this application[4,5].

Traditionally, muscles and bones were thought of as just biomechanical organs for the purpose of movement[6-8]. However, as the scientific field has advanced, so has the understanding that muscle and bone are also endocrine organs with the ability to regulate biological functions within their microenvironment[9]. Furthermore, muscle-bone interactions are much more diverse and complex than originally thought, transmitting not only biomechanical signals but biochemical signals as well[10-12].

The recent advances in the understanding of the complex biology of the musculoskeletal system have paved the way for improved *ex-vivo* and *in-vivo* imaging. The Fast Free-of-Acrylamide Clearing Tissue (FACT)[13,14] and CLARITY[15] techniques in *ex-vivo* imaging have recently been developed to elucidate three-dimensional skeletal muscle imaging, portraying a more comprehensive map of cellular interactions between neighboring and distant cells within skeletal muscle. Advancement of *in-vivo* imaging approaches, ranging from dynamic ultrasound imaging (US) to positron emission tomography (PET) have brought up novel possibilities of non-invasive anatomical and physiologic imaging for various clinical applications.

In this review, we summarize a range of *ex-vivo* and *in-vivo* imaging approaches related

Corresponding Author: Majid Assadi, MD; e-mail: Assadipoya@yahoo.com

to muscle and bone with an emphasis on recent progress made with new technologies, including three-dimensional imaging, US, magnetic resonance imaging (MRI), computed tomography (CT), and PET. It is our hope that structural imaging of muscles and bones may give novel insights into the diagnosis, treatment, and prevention of musculoskeletal diseases.

Methods

A systemic review and analysis of muscle and bone imaging studies published between January 1, 1950 and August 1, 2018 was performed using PubMed, Google Scholar, Web of Science, and Geen Medical database, following systematic review and meta-analysis guidelines[16]. The search terms used were bone, skeleton, orthopedics, osseous, osteology, muscle, muscular, skeletal muscle, imaging, two-dimensional imaging, three-dimensional imaging, CLARITY, FACT, US, MRI, CT, and PET. All studies, with no language restrictions and no species limitations, were included. Basic science and clinical *ex-vivo* and *in-vivo* studies ranging from randomized trials to retrospective studies were included (Tables I and II). Review, systematic review, meta-analyses, and unpublished doctoral theses were excluded. Investigators independently searched through the studies, if the eligibility of an article was inconsistent among two investigators, it was resolved by discussion and consensus.

Ex Vivo Imaging of the Muscle and Bone

Two-dimensional imaging

Two-dimensional imaging is the most common classical approach for studying the morphology of muscle[17,18] and bone[19,20] by taking thin sections of tissue and applying conventional staining approaches (Figure 1A), immunohistochemistry[21], immunofluorescence[22], electron microscopy[23], and *in situ* hybridization[24]. Studies applying these imaging methods have revealed the basic framework of muscle and bone with unbiased stereological and robust statistical methods.

Serial sectioning with these two-dimensional imaging techniques illustrate fine perspectives of structures within muscle and bone specimens. However, they do not fully characterize musculoskeletal interactions on a system level. Moreover, immunostaining and *in situ* hybridization were initially developed, and better optimized for soft tissues, such as the brain, instead of hard tissues, such as muscle and bone[25,26]. A major limitation facing these techniques is the ability to investigate intact muscular and osseous tissue, as well as their 3D microenvironments.

Three-Dimensional Imaging

Histological analyses at either light or electron microscopic levels are restricted to two dimensions. With these methods, it is challenging to reconstruct the exact structures of entire bone or muscle or investigate relationships among diverse musculoskeletal structures. With the synchro-

Table I. *Ex-vivo* muscle and bone imaging methods in basic and clinical studies.

Species	Immuno-histochemistry	Immuno-fluorescence	Electron microscope	CLARITY	*In situ* hybridization
Muscle					
Human	+[72]	+[22]	+[73]	–	+[74]
Mouse	+[21,75]	+[22]	+[23,76]	+[15]	+[77]
Rat	+[78]	+[22]	+[79]	–	–
Chicken	+[80]	+[81]	+[82]	–	+[83]
Dog	+[84]	+[85]	+[84]	–	–
Sheep	+[86]	–	+[87]	–	+[88]
Cattle	+[84,89]	+[90,91]	+[84,92]	–	+[93]
Bone					
Human	+[94]	+[95]	+[96]	–	+[97]
Mouse	+[98]	+[99]	+[100]	+[31]	+[98]
Rat	+[101]	+[102]	+[103]	–	+[104]
Sheep	+[105]	–	+[106]	–	–

+, it has been applied; -, it has not been applied.

Table II. *In-vivo* muscle and bone imaging methods in basic and clinical studies.

Species	US	MRI	CT	OCT	PET
Muscle					
Human	+[107,108]	+[109]	+[110]	+[111]	+[112-116]
Mouse	+[117]	+[118]	+[119]	+[120]	+[119]
Rat	+[121]	+[122]	–	+[123]	+[124]
Dog	+[125]	+[126]	+[127]	–	+[128]
Sheep	+[129]	+[130]	+[131]	+[132]	–
Pig	+[129]	+[133]	+[134]	+[135,136]	+[37]
Cattle	+[129,138]	+[139]	+[140,141]	+[142]	–
Bone					
Human	+[143]	+[144]	+[145,146]	+[147]	+[116]
Mouse	+[148]	+[149]	+[50]	+[151]	+[152]
Rat	+[153]	+[154]	+[155]	+[156]	+[157]
Dog	+[158]	+[159]	+[160]	+[161]	+[152]
Sheep	+[162]	–	+[131]	+[163]	–
Pig	+[164]	+[165]	+[166]	+[167]	+[168]

+, It has been applied; -, It has not been applied; US, ultrasound; MRI, magnetic resonance imaging; CT, computed tomography; OCT, optical coherence tomography; PET, positron emission tomography.

tron X-ray microtomography and 3D X-ray microscopy approach, imaging of musculoskeletal structures in fixed mouse bone or muscle without clearing has been done. However, these facilities are not widely accessible.

Three-dimensional imaging has recently attracted considerable attention due to advantages it can provide with detailed imaging of structural information of organs[27-29]. The CLARITY approach, developed by Chung and Deisseroth[30], elucidates the 3D cellular connectome and of intact tissue imaging. Zhang et al[15] based on the CLARITY technique has proven this approach to be successful in the whole muscle imaging of mice, facilitating connectomics and structural analyses within muscle vessels and cells in three-dimensional systems. Around the same period, Greenbaum et al[31] demonstrated comprehensive visualization of biological processes in the entire bone tissues with CLARITY (Figure 1B).

Recently, an exciting new wave of improvements emerged with free-of-acrylamide clearing tissue (FACT)[32], which greatly reduces the whole clearing time. Most notably, the replacement of acrylamide hydrogel by formaldehyde largely

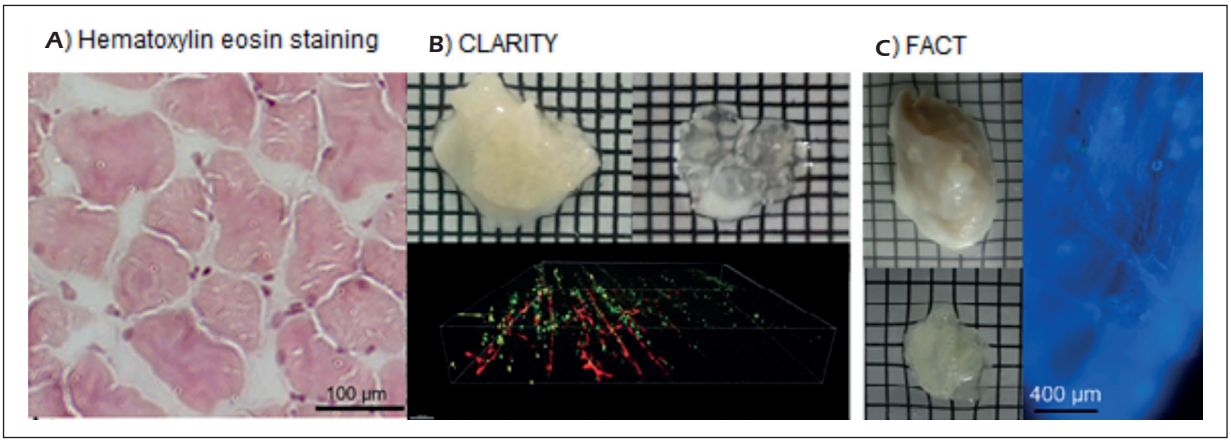

Figure 1. Imaging of ex-vivo muscular tissues. **A**, Hematoxylin and eosin staining of a muscle section of a rat (100X)[64]. **B**, Three-dimensional imaging of mouse muscle cleared with the passive CLARITY protocol. Blood vessels (red) and neurons (green and yellow) are labeled[15]. C, Imaging of skeletal muscle in the mouse after clearing by Fast Free-of-Acrylamide Clearing Tissue (FACT) technique and labeling with Hoechst 33342 (blue), the red and green are control without labeling[13].

avoids incomplete tissue hydrogel hybridization and fine cyst structure destruction in this protocol. Compared to other protocols, FACT improves the speed of clearing, preservation of cytoarchitecture, depth of tissue penetration, long-term storage of fluorescent signal, and the signal to noise ratio (Figure 1C).

The near-infrared (NIR) approach allows the visualization of follicle-stimulating hormone (FSH) receptors by conjugating FSH to a small molecule weight near-infrared fluorophore (CH1055). The strong near-infrared signals emitted from the fluorophore conjugated to FSH allow for the imaging of bones which express the FSH receptors[33]. Because the CH1055 fluorophore has minimal cytotoxicity and a short *in vivo* half-life[34], further improvements of the NIR approach and design of a portable NIR probe may potentially allow for live imaging of bone and muscle in patients as a diagnostic tool.

In Vivo Imaging of the Muscle and Bone

Ultrasonography

US imaging is a powerful empirical method in human and animal research to identify muscular and bone disorders. This technique involves sending and receiving a series of sound-wave pulses into biological tissues and analyzing acoustic and temporal properties of echoes for reconstructing structural imaging of tissues. Muscle thickness[35,36] and soft tissue changes adjacent to bone[37,38], often reflected by echo intensity can readily be identified using this method (Figures 2A and 3A). In addition, US offers the advantage of dynamic imaging, allowing for real-time visualization of muscle function and underlying pathologies.

Positron Emission Tomography

PET imaging allows for the observation of metabolic processes of tissues and organs[39,40].

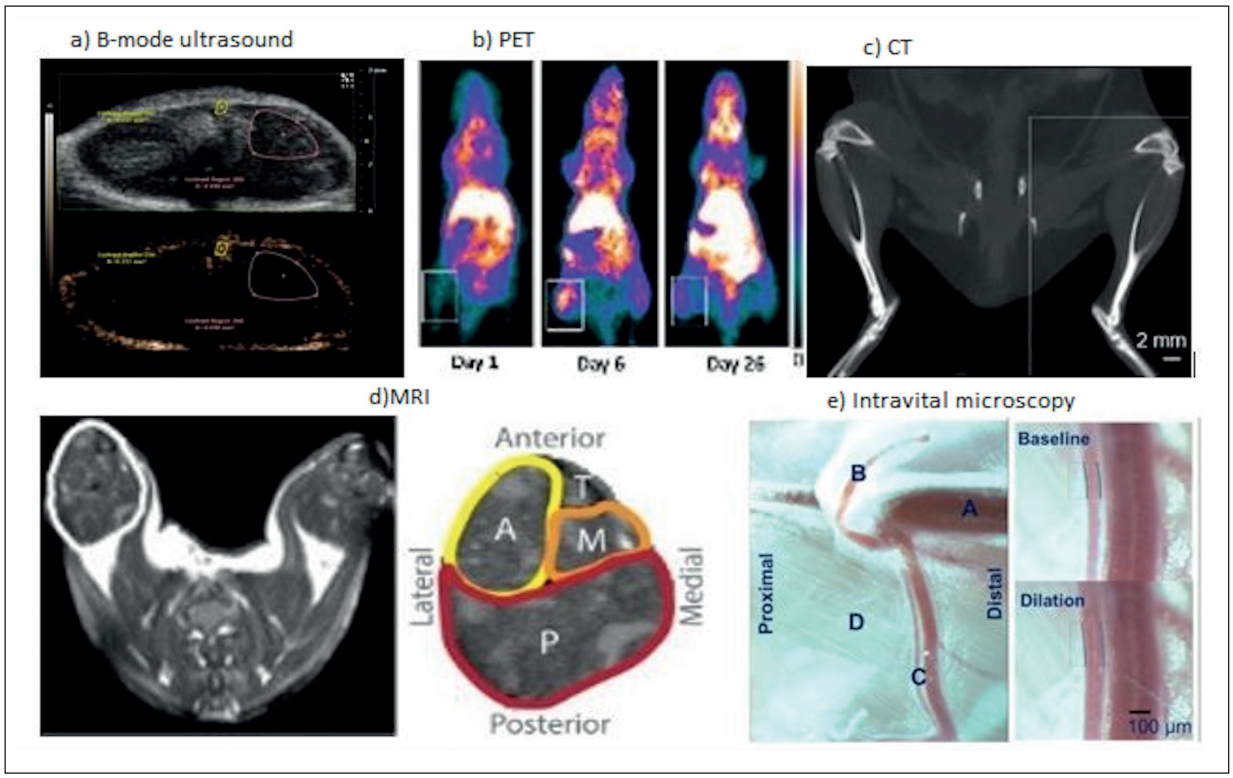

Figure 2. Different techniques for real-time live imaging of the muscle. **A**, B-mode contrast-enhanced ultrasonography imaging of muscle microvascular blood volume and femoral vessels in a mouse[65]. **B**, Positron emission tomography (PET) imaging of mouse muscular inflammation model. White boxes indicate inflammatory muscles[66]. **C**, Micro-computed tomography (CT) evaluation of the hind limb muscle mass in mice[67]. **D**, Magnetic resonance imaging (MRI) of leg shows changes in dystrophic muscle. The leg of the left hind limb outlined in white and a magnified version of the leg muscles; anterior muscle groups (A), medial muscle groups (M), posterior muscle groups (P), and the tibia bone (T)[68]. **E**, Intravital microscopic image of an adult mouse hind limb blood vessels. Femoral artery (A), epigastric artery (B), gracilis artery (C), and the adductor muscle (D)[65].

Dynamic biological processes mapping at high resolution in freely behaving patients and animals can be achieved by the detection of radioactivity emitted after radiotracer injection[41]. A wide array of radiotracers and clinical applications for PET imaging of the musculoskeletal system are under investigation, including the localization of dystonic muscles[42] and assessing for bone marrow lymphoma[43] (Figure 2B).

Computed Tomography

Computed tomography (CT) uses computer-processed incorporations of X-ray measurements to produce sectional images of specific tissues, including internal organs, soft tissue, muscle (Figure 2C), and bone (Figure 3B)[44-46]. CT allows for rapid anatomical imaging, and in some instances is the preferred imaging modality of the musculoskeletal system, such as in the imaging of acute trauma and post-operatively in the presence of metallic hardware. Additionally, CT-based imaging studies have helped extend previous work based on MRI in imaging muscle and bone morphological measurements[46,47].

Magnetic Resonance Imaging

Imaging with MRI applies a powerful magnetic field and radio waves to portray detailed images of the organs and tissues. Enormous advances have been made in improving this technique, including functional magnetic resonance imaging (fMRI) and real-time fMRI (rtfMRI). An investigation based on this approach provides reliable scan diagnosis in musculoskeletal diseases, such

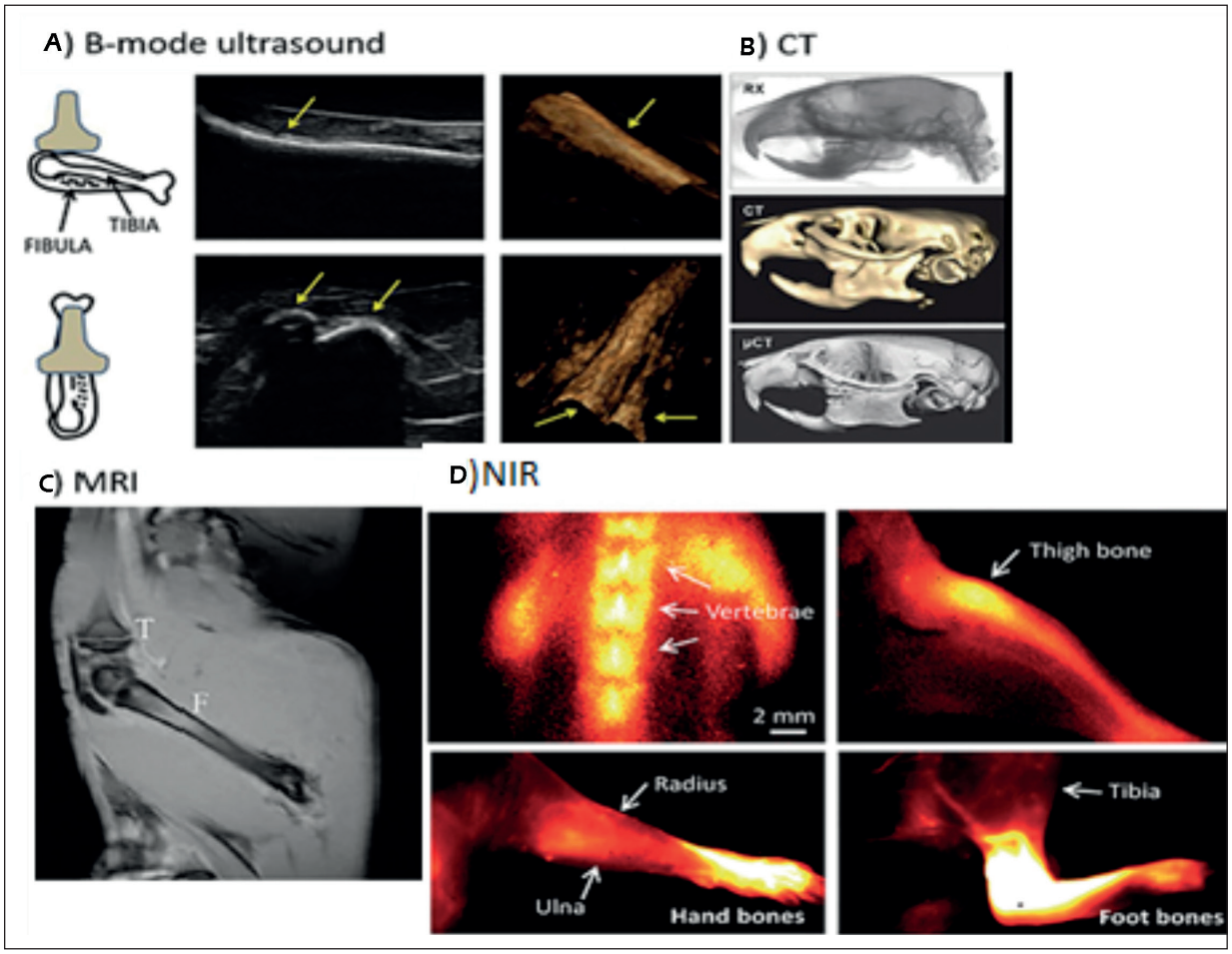

Figure 3. Different techniques for real-time live imaging of the bone. **A**, B-mode ultrasound imaging showing an intact tibia specimen (arrow) of chicken with the soft tissue left intact and 3D renditions of the chicken tibia[69]. **B**, Micro-computed tomography (μCT) evaluation of lateral view, left, of a mice skull comparing with simple radiology (RX) and conventional computed tomography (CT)[70]. **C**, Magnetic resonance imaging (MRI) of bone with contrast-enhanced (Gd-DTPA) T1-weighted MRI of a rat. The proximal tibia (T) and whole femur (F)[71]. **D**, Near-infrared (NIR) optical imaging of bones using follicle stimulating hormone-fluorophore CH1055 (FSH-CH) in adult mice[33].

as muscle and tendon injuries[48], degenerative and inflammatory arthropathies[49], and radiologic occult fractures[50] (Figures 2D and 3C).

Optical Coherence Tomography

Optical coherence tomography (OCT) is an in vivo imaging method based on low-coherence interferometry, typically employing near-infrared light, used for the evaluation of bones and muscles[51,52]. OCT is based on low-coherence interferometry, typically employing near-infrared light. The use of relatively long wavelength light allows it to penetrate into the scattering medium. This approach provides cross-sectional views of the subsurface microstructure of biological tissues. To decrease the effect of tissue motion (breathing or muscle contraction) during live imaging with OCT, an OCT system with higher imaging speed has been recommended[53], including the Fourier domain mode-locking laser[54] or an OCT A-line rate at the MHz level[55]. The OCT approach, however, suffers from the generation and interference of partially coherent optical fields and from how such fields propagate in biological tissues. In addition, there are issues related to the design of practical scanning and detection systems, which need to be overcomed before OCT will have practical clinical applications.

Intravital Multiphoton Microscopy

As an experimental tool, intravital multiphoton microscopy allows imaging of living tissue up to about one millimeter in depth (Figures 2E and 3D). This imaging technique was recently used to monitor the diameter and blood flow of individual vessels[33] and has shown utility for the imaging of the muscular surface. However, this approach is restricted by the depth of the observable field and currently has limited clinical application.

Clinical Applications of Ex-Vivo and In-vivo Muscle and Bone Imaging

Different muscle and bone types harbor specialized physiological processes that are critical for modulating biomechanical and endocrine functions, such as cell proliferation and growth, blood vessel recruitment, neuronal signals, and bone remodeling[56-59]. There is tremendous progress in clarifying the function and malfunction of muscle and bone with the aid of contemporary *ex-vivo* and *in-vivo* imaging techniques. Studies employing these methods have revealed a large variety of musculoskeletal diseases, including muscle atrophy[60], fatty infiltration[61], muscular fibrosis[62], and osteoporosis[63].

However, imaging the changes in metabolic processes of the musculoskeletal system and the interactions between muscle and bone have so far revealed little information in both basic and clinical research, although these biological processes have been suggested *via* cell and molecular biology experiments. The development of tools to simultaneously map real-time live imaging of special tissues within the musculoskeletal system remains a pressing clinical concern, with the non-invasive *in vivo* imaging in diagnosing musculoskeletal pathophysiology holding promise for future clinical applications.

Conclusions

Both basic and clinical studies have led to an advanced understanding of the structural and functional basis of muscle and bone underlying the development of imaging techniques. Recently, developed *ex-vivo* and *in-vivo* tools further boosted the research on understanding the morphology of muscle and bone with unprecedented precision. However, more comprehensive physiological and pathological imaging of the muscle and bone, with disease-type and disease-stage specificity of these organs, are needed. Additionally, investigating the function of the whole musculoskeletal system and interaction between muscle and bone, rather than studying the separated organ morphology, provides a novel interesting frontier that awaits further exploration.

Conflict of Interests

No potential conflicts of interest relevant to this article exist.

References

1) Ibrahim T, Farolfi A, Mercatali L, Ricci M, Amadori D. Metastatic bone disease in the era of bone-targeted therapy: clinical impact. Tumori 2013; 99: 1-9.
2) Kley RA, Tarnopolsky MA, Vorgerd M. Creatine for treating muscle disorders. Cochrane Database Syst Rev 2013; 2013: Cd004760.
3) Ates F, Temelli Y, Yucesoy CA. Intraoperative experiments show relevance of inter-antagonistic mechanical interaction for spastic muscle's contribution to joint movement disorder. Clin Biomech 2014; 29: 943-949.
4) Hamaoka T, Madewell JE, Podoloff DA, Hortobagyi GN, Ueno NT. Bone imaging in metastatic breast cancer. J Clin Oncol 2004; 22: 2942-2953.

5) Kawamoto S, Imamoglu N, Gomez-Tames JD, Kita K, Yu W. Ultrasound imaging and semi-automatic analysis of active muscle features in electrical stimulation by optical flow. Conf Proc IEEE Eng Med Biol Soc 2014; 2014: 250-253.
6) Biewener AA. Biomechanics of mammalian terrestrial locomotion. Science 1990; 250: 1097-1103.
7) Pandy MG, Andriacchi TP. Muscle and joint function in human locomotion. Annu Rev Biomed Eng 2010; 12: 401-433.
8) Lanyon L, Baggott D. Mechanical function as an influence on the structure and form of bone. J Bone Joint Surg Am 1976; 58: 436-443.
9) Brotto M, Johnson ML. Endocrine crosstalk between muscle and bone. Curr Osteoporos Rep 2014; 12: 135-141.
10) Digirolamo DJ, Clemens TL, Kousteni S. The skeleton as an endocrine organ. Nat Rev Rheumatol 2012; 8: 674-683.
11) Karsenty G, Oury F. Biology without walls: the novel endocrinology of bone. Annu Rev Physiol 2012; 74: 87-105.
12) Brotto M, Bonewald L. Bone and muscle: Interactions beyond mechanical. Bone 2015; 80: 109-114.
13) Khoradmehr A, Mazaheri F, Anvari M, Tamadon A. A simple technique for three-dimensional imaging and segmentation of brain vasculature using Fast Free-of-Acrylamide Clearing Tissue (FACT) in murine. Cell J 2019; 21: 49-56.
14) Mohammad Rezazadeh F, Saedi S, Rahmanifar F, Namavar MR, Dianatpour M, Tanideh N, Akhlaghi A, Niazi A, Arabi Monfared A, Tsutsui K, Jafarzadeh Shirazi MR. Fast free of acrylamide clearing tissue (FACT) for clearing, immunolabeling and three-dimensional imaging of partridge tissues. Microsc Res Tech 2018; 81: 1374-1382.
15) Zhang W, Liu S, Zhang W, Hu W, Jiang M, Tamadon A, Feng Y. Skeletal muscle CLARITY: A preliminary study of imaging the three-dimensional architecture of blood vessels and neurons. Cell J 2018; 20: 132-137.
16) Liberati A, Altman DG, Tetzlaff J, Mulrow C, Gøtzsche PC, Ioannidis JP, Clarke M, Devereaux PJ, Kleijnen J, Moher D. The PRISMA statement for reporting systematic reviews and meta-analyses of studies that evaluate health care interventions: explanation and elaboration. J Clin Epidemiol 2009; 62: e1-34.
17) Mauro A. Satellite cell of skeletal muscle fibers. J Biophys Biochem Cytol 1961; 9: 493-495.
18) Damrauer JS, Stadler ME, Acharyya S, Baldwin AS, Couch ME, Guttridge DC. Chemotherapy-induced muscle wasting: association with NF-κB and cancer cachexia. Eur J Transl Myol 2018; 28.
19) Garrahan N, Mellish R, Compston J. A new method for the two-dimensional analysis of bone structure in human iliac crest biopsies. J Microsc 1986; 142: 341-349.
20) Yao G, Wang LV. Two-dimensional depth-resolved Mueller matrix characterization of biological tissue by optical coherence tomography. Opt Lett 1999; 24: 537-539.
21) Trittmann JK, Velten M, Heyob KM, Almazroue H, Jin Y, Nelin LD, Rogers LK. Arginase and α-smooth muscle actin induction after hyperoxic exposure in a mouse model of bronchopulmonary dysplasia. Clin Exp Pharmacol Physiol 2018; 45: 556-562.
22) Bloemberg D, Quadrilatero J. Rapid determination of myosin heavy chain expression in rat, mouse, and human skeletal muscle using multicolor immunofluorescence analysis. PLoS One 2012; 7: e35273.
23) Shafiq S, Gorycki M. Regeneration in skeletal muscle of mouse: some electron-microscope observations. J Pathol Bacteriol 1965; 90: 123-127.
24) Hogan MC, Arthur PG, Bebout DE, Hochachka PW, Wagner PD. Role of O2 in regulating tissue respiration in dog muscle working in situ. J Appl Physiol 1992; 73: 728-736.
25) Chung K, Wallace J, Kim SY, Kalyanasundaram S, Andalman AS, Davidson TJ, Mirzabekov JJ, Zalocusky KA, Mattis J, Denisin AK, Pak S. Structural and molecular interrogation of intact biological systems. Nature 2013; 497: 332-337.
26) Susaki EA, Ueda HR. Whole-body and whole-organ clearing and imaging techniques with single-cell resolution: toward organism-level systems biology in mammals. Cell Chem Biol 2016; 23: 137-157.
27) Richardson DS, Lichtman JW. Clarifying tissue clearing. Cell 2015; 162: 246-257.
28) Susaki EA, Tainaka K, Perrin D, Kishino F, Tawara T, Watanabe TM, Yokoyama C, Onoe H, Eguchi M, Yamaguchi S, Abe T, Kiyonari H, Shimizu Y, Miyawaki A, Yokota H, Ueda HR. Whole-brain imaging with single-cell resolution using chemical cocktails and computational analysis. Cell J 2014; 157: 726-739.
29) Kim SY, Chung K, Deisseroth K. Light microscopy mapping of connections in the intact brain. Trends Cogn Sci 2013; 17: 596-599.
30) Chung K, Deisseroth K. CLARITY for mapping the nervous system. Nat Methods 2013; 10: 508-513.
31) Greenbaum A, Chan KY, Dobreva T, Brown D, Balani DH, Boyce R, Kronenberg HM, McBride HJ, Gradinaru V. Bone CLARITY: clearing, imaging, and computational analysis of osteoprogenitors within intact bone marrow. Sci Transl Med 2017; 9. pii: eaah6518.
32) Xu N, Tamadon A, Liu Y, Ma T, Leak RK, Chen J, Gao Y, Feng Y. Fast free-of-acrylamide clearing tissue (FACT)-an optimized new protocol for rapid, high-resolution imaging of three-dimensional brain tissue. Sci Rep 2017; 7: 9895.
33) Feng Y, Zhu S, Antaris AL, Chen H, Xiao Y, Lu X, Jiang L, Diao S, Yu K, Wang Y, Herraiz S. Live imaging of follicle stimulating hormone receptors in gonads and bones using near infrared II fluorophore. Chem Sci 2017; 8: 3703-3711.
34) Antaris AL, Chen H, Cheng K, Sun Y, Hong G, Qu C, Diao S, Deng Z, Hu X, Zhang B, Zhang X. A small-molecule dye for NIR-II imaging. Nat Mater 2016; 15: 235-242.
35) Kawai H, Kera T, Hirayama R, Hirano H, Fujiwara Y, Ihara K, Kojima M, Obuchi S. Morphological and qualitative characteristics of the quadriceps muscle of community-dwelling older adults based on ultrasound imaging: classification using latent class analysis. Aging Clin Exp Res 2018; 30: 283-291.
36) McKenna LJ, de Ronde M, Le M, Burke W, Graves A, Williams SA. Measurement of muscle thickness of the serratus anterior and lower trapezius using

ultrasound imaging in competitive recreational adult swimmers, with and without current shoulder pain. J Sci Med Sport 2018; 21: 129-133.
37) Giles SL, Winfield JM, Collins DJ, Rivens I, Civale J, ter Haar GR, deSouza NM. Value of diffusion-weighted imaging for monitoring tissue change during magnetic resonance-guided high-intensity focused ultrasound therapy in bone applications: an ex-vivo study. Eur Radiol Exp 2018; 2: 10.
38) Jakubovic R, Ramjist J, Gupta S, Guha D, Sahgal A, Foster FS, Yang VX. High-frequency micro-ultrasound imaging and optical topographic imaging for spinal surgery: initial experiences. Ultrasound Med Biol 2018; 44: 2379-2387.
39) Wolk DA, Sadowsky C, Safirstein B, Rinne JO, Duara R, Perry R, Agronin M, Gamez J, Shi J, Ivanoiu A, Minthon L. Use of flutemetamol F 18–labeled positron emission tomography and other biomarkers to assess risk of clinical progression in patients with amnestic mild cognitive impairment. JAMA Neurol 2018; 75: 1114-1123.
40) Gallamini A, Tarella C, Viviani S, Rossi A, Patti C, Mulé A, Picardi M, Romano A, Cantonetti M, La Nasa G, Trentin L. Early chemotherapy intensification with escalated BEACOPP in patients with advanced-stage Hodgkin lymphoma with a positive interim positron emission tomography/computed tomography scan after two ABVD cycles: Long-term results of the GITIL/FIL HD 0607 trial. J Clin Oncol 2018; 36: 454-462.
41) Berger A. Positron emission tomography. Br Med J 2003; 326: 1449.
42) Shen Y, Hu Y, Cai L, Li B, Pan L, Jin L. Localization of dystonic muscles with positron emission tomography/computed tomography for the treatment of cervical dystonia. J Nucl Med 2018; 46: e56.
43) Moritani K, Nakano N, Yonezawa S, Ochi F, Tauchi H, Eguchi-Ishimae M, Eguchi M, Ishii E, Nagai K. Usefulness of positron emission tomography-CT for diagnosis of primary bone marrow lymphoma in children. Pediatr Hematol Oncol 2018; 12: 1-6.
44) Wang LV. Multiscale photoacoustic microscopy and computed tomography. Nat Photonics 2009; 3: 503-509.
45) Martin L, Hopkins J, Malietzis G, Jenkins JT, Sawyer MB, Brisebois R, MacLean A, Nelson G, Gramlich L, Baracos VE. Assessment of computed tomography (CT)-defined muscle and adipose tissue features in relation to short-term outcomes after elective surgery for colorectal cancer: a multicenter approach. Ann Surg Oncol 2018; 25: 2669-2680.
46) Adams GJ, Cook RB, Hutchinson JR, Zioupos P. Bone apparent and material densities examined by cone beam computed tomography and the Archimedes technique: comparison of the two methods and their results. Front Mech Eng 2018; 3: 23.
47) Reeves JM, Knowles NK, Athwal GS, Johnson JA. Methods for post hoc quantitative computed tomography bone density calibration: Phantom-only and regression. J Biomech Eng 2018; 140: 094501
48) Gejo R, Kawaguchi Y, Kondoh T, Tabuchi E, Matsui H, Torii K, Ono T, Kimura T. Magnetic resonance imaging and histologic evidence of postoperative back muscle injury in rats. Spine 2000; 25: 941-946.
49) Haavardsholm EA, Bøyesen P, Østergaard M, Schildvold A, Kvien TK. Magnetic resonance imaging findings in 84 patients with early rheumatoid arthritis: bone marrow oedema predicts erosive progression. Ann Rheum Dis 2008; 67: 794-800.
50) Rizzo PF, Gould ES, Lyden JP, Asnis SE. Diagnosis of occult fractures about the hip. Magnetic resonance imaging compared with bone-scanning. J Bone Joint Surg Am 1993; 75: 395-401.
51) Lovering RM, Shah SB, Pratt SJ, Gong WEI, Chen YU. Architecture of healthy and dystrophic muscles detected by optical coherence tomography. Muscle Nerve 2013; 47: 588-590.
52) Bernstein L, Beaudette K, Patten K, Beaulieu-Ouellet É, Strupler M, Moldovan F, Boudoux C. Non-invasive imaging of zebrafish with spinal deformities using optical coherence tomography: a preliminary study. Paper presented at: Photonic Therapeutics and Diagnostics IX2013; San Francisco, California, United States.
53) Burton JC, Wang S, Stewart CA, Behringer RR, Larina IV. High-resolution three-dimensional in vivo imaging of mouse oviduct using optical coherence tomography. Biomed Opt Express 2015; 6: 2713-2723.
54) Huber R, Wojtkowski M, Fujimoto JG. Fourier Domain Mode Locking (FDML): a new laser operating regime and applications for optical coherence tomography. Opt Express 2006; 14: 3225-3237.
55) Klein T, Wieser W, Reznicek L, Neubauer A, Kampik A, Huber R. Multi-MHz retinal OCT. Biomed Opt Express 2013; 4: 1890-1908.
56) Bianco P, Robey PG. Skeletal stem cells. Development 2015;142(6):1023-1027.
57) Morrison SJ, Scadden DT. The bone marrow niche for haematopoietic stem cells. Nature 2014; 505: 327-334.
58) Rachner TD, Khosla S, Hofbauer LC. Osteoporosis: now and the future. Lancet 2011; 377: 1276-1287.
59) Lo CC, Chiang AS. Toward whole-body connectomics. J Neurosci 2016; 36: 11375-11383.
60) Bus SA, Yang QX, Wang JH, Smith MB, Wunderlich R, Cavanagh PR. Intrinsic muscle atrophy and toe deformity in the diabetic neuropathic foot: a magnetic resonance imaging study. Diabetes Care 2002; 25: 1444-1450.
61) Elliott J, Jull G, Noteboom JT, Darnell R, Galloway G, Gibbon WW. Fatty infiltration in the cervical extensor muscles in persistent whiplash-associated disorders: a magnetic resonance imaging analysis. Spine 2006; 31: E847-E855.
62) Tandon A, Villa CR, Hor KN, Jefferies JL, Gao Z, Towbin JA, Wong BL, Mazur W, Fleck RJ, Sticka JJ, Benson DW. Myocardial fibrosis burden predicts left ventricular ejection fraction and is associated with age and steroid treatment duration in Duchenne muscular dystrophy. J Am Heart Assoc 2015; 4. pii: e001338.
63) Link TM. Osteoporosis imaging: state of the art and advanced imaging. Radiology 2012; 263: 3-17.
64) Marella M, Seo BB, Flotte TR, Matsuno-Yagi A, Yagi T. No immune responses by the expression of the yeast Ndi1 protein in rats. PLoS One 2011; 6: e25910.
65) Turaihi AH, van Poelgeest EM, van Hinsbergh VWM, Serné EH, Smulders YM, Eringa EC. Combined

intravital microscopy and contrast-enhanced ultrasonography of the mouse hindlimb to study insulin-induced vasodilation and muscle perfusion. J Vis Exp 2017; 121: 54912.
66) Wu C, Yue X, Lang L, Kiesewetter DO, Li F, Zhu Z, Niu G, Chen X. Longitudinal PET imaging of muscular inflammation using(18)F-DPA-714 and (18)F-alfatide II and differentiation with tumors. Theranostics 2014; 4: 546-555.
67) Pasetto L, Olivari D, Nardo G, Trolese MC, Bendotti C, Piccirillo R, Bonetto V. Micro-computed tomography for non-invasive evaluation of muscle atrophy in mouse models of disease. PLoS One 2018; 13: e0198089.
68) Heier CR, Guerron AD, Korotcov A, Lin S, Gordish-Dressman H, Fricke S, Sze RW, Hoffman EP, Wang P, Nagaraju K. Non-Invasive MRI and spectroscopy of mdx mice reveal temporal changes in dystrophic muscle imaging and in energy deficits. PLoS One 2014; 9: e112477.
69) Parmar BJ, Chaudhry A, Weiner BK, Sabonghy EP, Tasciotti E, Righetti R. Real-time ultrasound imaging of complex skeletal defects and fractures preliminary results. Imaging Med 2017; 9: 19-28.
70) de Carlos F, Alvarez-Suárez A, Costilla S, Noval I, Vega JA, Cobo J. 3D-μCT cephalometric measurements in mice. Computed Tomography-Special Applications, In Tech Open 2011: 10-5772.
71) Doré-Savard L, Otis V, Belleville K, Lemire M, Archambault M, Tremblay L, Beaudoin JF, Beaudet N, Lecomte R, Lepage M, Gendron L. Behavioral, medical imaging and histopathological features of a new rat model of bone cancer pain. PLoS One 2010; 5: e13774.
72) D'Lugos AC, Patel SH, Fry CS, Carroll CC, Dickinson JM. Differential response of mTOR and ERK signaling in human skeletal muscle following resistance exercise and acetaminophen consumption. FASEB J 2018; 32(1_supplement): lb247-lb247.
73) Ogata T, Yamasaki Y. Ultra-high-resolution scanning electron microscopy of mitochondria and sarcoplasmic reticulum arrangement in human red, white, and intermediate muscle fibers. Anat Rec 1997; 248: 214-223.
74) Müller-Höcker J, Seibel P, Schneiderbanger K, Kadenbach B. Different in situ hybridization patterns of mitochondrial DNA in cytochrome c oxidase-deficient extraocular muscle fibres in the elderly. Virchows Arch A Pathol Anat Histopathol 1993; 422: 7-15.
75) Levy M, Barron L, Meyer K, Szoka JF. Characterization of plasmid DNA transfer into mouse skeletal muscle: evaluation of uptake mechanism, expression and secretion of gene products into blood. Gene Ther 1996; 3: 201-211.
76) Martins AR, Crisma AR, Masi LN, Amaral CL, Marzuca-Nassr GN, Bomfim LH, Teodoro BG, Queiroz AL, Serdan TD, Torres RP, Mancini-Filho J. Attenuation of obesity and insulin resistance by fish oil supplementation is associated with improved skeletal muscle mitochondrial function in mice fed a high-fat diet. J Nutr Biochem 2018; 55: 76-88.
77) Bhagwati S, Ghatpande A, Shafiq S, Leung B. In situ hybridization analysis for expression of myogenic regulatory factors in regenerating muscle of mdx mouse. J Neuropathol Exp Neurol 1996; 55: 509-514.
78) Smerdu V, Perše M. Effect of high-fat mixed lipid diet and swimming on fibre types in skeletal muscles of rats with colon tumours. Eur J Histochem 2018; 62: 2945.
79) Karnovsky MJ. The localization of cholinesterase activity in rat cardiac muscle by electron microscopy. J Cell Biol 1964; 23: 217-232.
80) Sartore S, Pierobon-Bormioli S, Schiaffino S. Immunohistochemical evidence for myosin polymorphism in the chicken heart. Nature 1978; 274: 82-83.
81) Sweeney LJ, Clark WA, Umeda PK, Zak R, Manasek FJ. Immunofluorescence analysis of the primordial myosin detectable in embryonic striated muscle. Proc Natl Acad Sci USA 1984; 81: 797-800.
82) Tokuyasu K, Dutton AH, Geiger B, Singer S. Ultrastructure of chicken cardiac muscle as studied by double immunolabeling in electron microscopy. Proc Natl Acad Sci USA 1981; 78: 7619-7623.
83) Singer RH, Ward DC. Actin gene expression visualized in chicken muscle tissue culture by using in situ hybridization with a biotinated nucleotide analog. Proc Natl Acad Sci USA 1982; 79: 7331-7335.
84) Peters M, Lütkefels E, Heckeroth A, Schares G. Immunohistochemical and ultrastructural evidence for Neospora caninum tissue cysts in skeletal muscles of naturally infected dogs and cattle. Int J Parasitol 2001; 31: 1144-1148.
85) Shelton GD, Liu LA, Guo LT, Smith GK, Christiansen JS, Thomas WB, Smith MO, Kline KL, March PA, Flegel T, Engvall E. Muscular dystrophy in female dogs. J Vet Intern Med 2001; 15: 240-244.
86) Bünger L, Navajas EA, Stevenson L, Lambe NR, Maltin CA, Simm G, Fisher AV, Chang KC. Muscle fibre characteristics of two contrasting sheep breeds: Scottish blackface and texel. Meat Sci 2009; 81: 372-381.
87) Gerber C, Meyer DC, Frey E, von Rechenberg B, Hoppeler H, Frigg R, Jost B, Zumstein MA. Neer Award 2007: reversion of structural muscle changes caused by chronic rotator cuff tears using continuous musculotendinous traction. An experimental study in sheep. J Shoulder Elbow Surg 2009; 18: 163-171.
88) Kershaw CM, Scaramuzzi RJ, McGowan MR, Wheeler-Jones CP, Khalid M. The expression of prostaglandin endoperoxide synthase 2 messenger RNA and the proportion of smooth muscle and collagen in the sheep cervix during the estrous cycle. Biol Reprod 2007; 76: 124-129.
89) Nakano T, Li X, Sunwoo H, Sim J. Immunohistochemical localization of proteoglycans in bovine skeletal muscle and adipose connective tissues. Can J Anim Sci 1997; 77: 169-172.
90) Fritz JD, Greaser ML. Changes in titin and nebulin in postmortem bovine muscle revealed by gel electrophoresis, western blotting and immunofluorescence microscopy. J Food Sci 1991; 56: 607-610.
91) Duarte MS, Paulino PV, Das AK, Wei S, Serao NV, Fu X, Harris SM, Dodson MV, Du M. Enhancement of adipogenesis and fibrogenesis in skeletal muscle of Wagyu compared with Angus cattle. J Anim Sci 2013; 91: 2938-2946.

92) Jones SB, Carroll RJ, Cavanaugh JR. Structural changes in heated bovine muscle: a scanning electron microscope study. J Food Sci 1977; 42: 125-131.
93) Hayes H, Petit E, Bouniol C, Popescu P. Localization of the α-S2-casein gene (CASAS2) to the homoeologous cattle, sheep, and goat chromosomes 4 by in situ hybridization. Cytogenet Genome Res 1993; 64: 281-285.
94) Beckstead JH, Halverson PS, Ries CA, Bainton DF. Enzyme histochemistry and immunohistochemistry on biopsy specimens of pathologic human bone marrow. Blood 1981; 57: 1088-1098.
95) Pal R, Venkataramana NK, Bansal A, Balaraju S, Jan M, Chandra R, Dixit A, Rauthan A, Murgod U, Totey S. Ex vivo-expanded autologous bone marrow-derived mesenchymal stromal cells in human spinal cord injury/paraplegia: a pilot clinical study. Cytotherapy 2009; 11: 897-911.
96) Boström K, Watson K, Horn S, Wortham C, Herman I, Demer L. Bone morphogenetic protein expression in human atherosclerotic lesions. J Clin Invest 1993; 91: 1800-1809.
97) Sungaran R, Markovic B, Chong B. Localization and regulation of thrombopoietin mRNA expression in human kidney, liver, bone marrow, and spleen using in situ hybridization. Blood 1997; 89: 101-107.
98) Shibata S, Fukada K, Suzuki S, Ogawa T, Yamashita Y. In situ hybridization and immunohistochemistry of bone sialoprotein and secreted phosphoprotein 1 (osteopontin) in the developing mouse mandibular condylar cartilage compared with limb bud cartilage. J Anat 2002; 200: 309-320.
99) Gil-Henn H, Destaing O, Sims NA, Aoki K, Alles N, Neff L, Sanjay A, Bruzzaniti A, De Camilli P, Baron R, Schlessinger J. Defective microtubule-dependent podosome organization in osteoclasts leads to increased bone density in Pyk2–/– mice. J Cell Biol 2007; 178: 1053-1064.
100) Hughes L, Archer C, Ap Gwynn I. The ultrastructure of mouse articular cartilage: collagen orientation and implications for tissue functionality. A polarised light and scanning electron microscope study and review. Eur Cell Mater 2005; 9: e84.
101) Erben RG. Embedding of bone samples in methylmethacrylate: an improved method suitable for bone histomorphometry, histochemistry, and immunohistochemistry. J Histochem Cytochem 1997; 45: 307-313.
102) Mark MP, Prince CW, Oosawa T, Gay S, Bronckers AL, Butler WT. Immunohistochemical demonstration of a 44-KD phosphoprotein in developing rat bones. J Histochem Cytochem 1987; 35: 707-715.
103) Weiss L. The structure of bone marrow. Functional interrelationships of vascular and hematopoietic compartments in experimental hemolytic anemia: an electron microscopic study. J Morphol 1965; 117: 467-537.
104) Chen J, Shapiro HS, Wrana JL, Reimers S, Heersche JN, Sodek J. Localization of bone sialoprotein (BSP) expression to sites of mineralized tissue formation in fetal rat tissues by in situ hybridization. Matrix 1991; 11: 133-143.
105) Lovric V, Ledger M, Goldberg J, Harper W, Bertollo N, Pelletier MH, Oliver RA, Yu Y, Walsh WR. The effects of low-intensity pulsed ultrasound on tendon-bone healing in a transosseous-equivalent sheep rotator cuff model. Knee Surg Sports Traumatol Arthrosc 2013; 21: 466-475.
106) Le Nihouannen D, Daculsi G, Saffarzadeh A, Gauthier O, Delplace S, Pilet P, Layrolle P. Ectopic bone formation by microporous calcium phosphate ceramic particles in sheep muscles. Bone 2005; 36: 1086-1093.
107) Narici M, Cerretelli P. Changes in human muscle architecture in disuse-atrophy evaluated by ultrasound imaging. J Gravit Physiol 1998; 5: P73-P74.
108) Bakke M, Tuxetv A, Vilmann P, Jensen BR, Vilmann A, Toft M. Ultrasound image of human masseter muscle related to bite force, electromyography, facial morphology, and occlusal factors. Eur J Oral Sci 1992; 100: 164-171.
109) Lansdown DA, Ding Z, Wadington M, Hornberger JL, Damon BM. Quantitative diffusion tensor MRI-based fiber tracking of human skeletal muscle. J Appl Physiol 2007; 103: 673-681.
110) Giusto M, Lattanzi B, Albanese C, Galtieri A, Farcomeni A, Giannelli V, Lucidi C, Di Martino M, Catalano C, Merli M. Sarcopenia in liver cirrhosis: the role of computed tomography scan for the assessment of muscle mass compared with dual-energy X-ray absorptiometry and anthropometry. Eur J Gastroenterol Hepatol 2015; 27: 328-334.
111) Nadkarni SK, Pierce MC, Park BH, de Boer JF, Whittaker P, Bouma BE, Bressner JE, Halpern E, Houser SL, Tearney GJ. Measurement of collagen and smooth muscle cell content in atherosclerotic plaques using polarization-sensitive optical coherence tomography. J Am Coll Cardiol 2007; 49: 1474-1481.
112) Tashiro M, Fujimoto T, Itoh M, Kubota K, Fujiwara T, Miyake M, Watanuki S, Horikawa E, Sasaki H, Ido T. 18F-FDG PET imaging of muscle activity in runners. J Nucl Med 1999; 40: 70-76.
113) Pappas GP, Olcott EW, Drace JE. Imaging of skeletal muscle function using 18FDG PET: force production, activation, and metabolism. J Appl Physiol 2001; 90: 329-337.
114) Tearney G, Brezinski M, Southern J, Bouma B, Hee M, Fujimoto J. Determination of the refractive index of highly scattering human tissue by optical coherence tomography. Opt Lett 1995; 20: 2258-2260.
115) Kemppainen J, Fujimoto T, Kalliokoski KK, Viljanen T, Nuutila P, Knuuti J. Myocardial and skeletal muscle glucose uptake during exercise in humans. J Physiol (Lond) 2002; 542: 403-412.
116) Nuutila P, Knuuti MJ, Mäki M, Laine H, Ruotsalainen U, Teräs M, Haaparanta M, Solin O, Yki-Järvinen H. Gender and insulin sensitivity in the heart and in skeletal muscles: studies using positron emission tomography. Diabetes 1995; 44: 31-36.
117) Chappell JC, Klibanov AL, Price RJ. Ultrasound-microbubble-induced neovascularization in mouse skeletal muscle. Ultrasound Med Biol 2005; 31: 1411-1422.
118) Samagh SP, Kramer EJ, Melkus G, Laron D, Bodendorfer BM, Natsuhara K, Kim HT, Liu X, Feeley BT.

MRI quantification of fatty infiltration and muscle atrophy in a mouse model of rotator cuff tears. J Orthop Res 2013; 31: 421-426.
119) Nahrendorf M, Zhang H, Hembrador S, Panizzi P, Sosnovik DE, Aikawa E, Libby P, Swirski FK, Weissleder R. Nanoparticle PET-CT imaging of macrophages in inflammatory atherosclerosis. Circulation 2008; 117: 379-387.
120) Yang X, Lorenser D, McLaughlin RA, Kirk RW, Edmond M, Simpson MC, Grounds MD, Sampson DD. Imaging deep skeletal muscle structure using a high-sensitivity ultrathin side-viewing optical coherence tomography needle probe. Biomed Opt Express 2014; 5: 136-148.
121) Leong-Poi H, Christiansen J, Heppner P, Lewis CW, Klibanov AL, Kaul S, Lindner JR. Assessment of endogenous and therapeutic arteriogenesis by contrast ultrasound molecular imaging of integrin expression. Circulation 2005; 111: 3248-3254.
122) Mahmoud-Ghoneim D, Cherel Y, Lemaire L, Jacques D, Maniere A. Texture analysis of magnetic resonance images of rat muscles during atrophy and regeneration. Magn Reson Imaging 2006; 24: 167-171.
123) De Boer JF, Srinivas SM, Park BH, Pham TH, Chen Z, Milner TE, Nelson JS. Polarization effects in optical coherence tomography of various biological tissues. IEEE J Sel Top Quantum Electron 1999; 5: 1200-1204.
124) Wu JC, Chen IY, Sundaresan G, Min JJ, De A, Qiao JH, Fishbein MC, Gambhir SS. Molecular imaging of cardiac cell transplantation in living animals using optical bioluminescence and positron emission tomography. Circulation 2003; 108: 1302-1305.
125) Pillen S, Tak RO, Zwarts MJ, Lammens MM, Verrijp KN, Arts IM, van der Laak JA, Hoogerbrugge PM, van Engelen BG, Verrips A. Skeletal muscle ultrasound: correlation between fibrous tissue and echo intensity. Ultrasound Med Biol 2009; 35: 443-446.
126) Kobayashi M, Nakamura A, Hasegawa D, Fujita M, Orima H, Takeda Si. Evaluation of dystrophic dog pathology by fat-suppressed T2-weighted imaging. Muscle Nerve 2009; 40: 815-826.
127) Rossmeisl Jr JH, Rohleder JJ, Hancock R, Lanz OI. Computed tomographic features of suspected traumatic injury to the iliopsoas and pelvic limb musculature of a dog. Vet Radiol Ultrasound 2004; 45: 388-392.
128) Madar I, Ravert HT, Du Y, Hilton J, Volokh L, Dannals RF, Frost JJ, Hare JM. Characterization of uptake of the new PET imaging compound 18F-fluorobenzyl triphenyl phosphonium in dog myocardium. J Nucl Med 2006; 47: 1359-1366.
129) McLaren DG, Novakofski J, Parrett DF, Lo LL, Singh SD, Neumann KR, McKeith FK. A study of operator effects on ultrasonic measures of fat depth and longissimus muscle area in cattle, sheep and pigs. J Anim Sci 1991; 69: 54-66.
130) Healy LJ, Jiang Y, Hsu EW. Quantitative comparison of myocardial fiber structure between mice, rabbit, and sheep using diffusion tensor cardiovascular magnetic resonance. J Cardiovasc Magn Reson 2011; 13: 74.
131) Aras MH, Miloglu O, Barutcugil C, Kantarci M, Ozcan E, Harorli A. Comparison of the sensitivity for detecting foreign bodies among conventional plain radiography, computed tomography and ultrasonography. Dentomaxillofac Radiol 2010; 39: 72.
132) Weaver B, Staddon G, Pearson M. Tissue blood content in anaesthetised sheep and horses. Comp Biochem Physiol A Comp Physiol 1989; 94: 401-404.
133) Monziols M, Collewet G, Bonneau M, Mariette F, Davenel A, Kouba M. Quantification of muscle, subcutaneous fat and intermuscular fat in pig carcasses and cuts by magnetic resonance imaging. Meat Sci 2006; 72: 146-154.
134) Font-i-Furnols M, Brun A, Tous N, Gispert M. Use of linear regression and partial least square regression to predict intramuscular fat of pig loin computed tomography images. Chemometr Intell Lab Syst 2013; 122: 58-64.
135) Yang Y, Wu L, Feng Y, Wang RK. Observations of birefringence in tissues from optic-fibre-based optical coherence tomography. Meas Sci Technol 2002; 14: 41.
136) Yang Y, Whiteman S, van Pittius DG, He Y, Wang RK, Spiteri MA. Use of optical coherence tomography in delineating airways microstructure: comparison of OCT images to histopathological sections. Phys Med Biol 2004; 49: 1247-1255.
137) Feldman HS, Hartvig P, Wiklund L, Doucette AM, Antoni G, Gee A, Ulin J, Langstrom B. Regional distribution of 11C-labeled lidocaine, bupivacaine, and ropivacaine in the heart, lungs, and skeletal muscle of pigs studied with positron emission tomography. Biopharm Drug Dispos 1997; 18: 151-164.
138) Shore D, Woods M, Miles C. Attenuation of ultrasound in post rigor bovine skeletal muscle. Ultrasonics 1986; 24: 81-87.
139) Wedeen VJ, Reese TG, Napadow VJ, Gilbert RJ. Demonstration of primary and secondary muscle fiber architecture of the bovine tongue by diffusion tensor magnetic resonance imaging. Biophys J 2001; 80: 1024-1028.
140) Raji AR, Sardari K, Mohammadi H. Normal cross–sectional anatomy of the bovine digit: comparison of computed tomography and limb anatomy. Anat Histol Embryol 2008; 37: 188-191.
141) Nade T, Fujita K, Fujii M, Yoshiba M, Haryu T, Misumi S, Okumura T. Development of X-ray computed tomography for live standing cattle. Anim Sci J 2005; 76: 513-517.
142) Fan C, Yao G. Imaging myocardial fiber orientation using polarization sensitive optical coherence tomography. Biomed Opt Express 2013; 4: 460-465.
143) Karjalainen JP, Töyräs J, Riekkinen O, Hakulinen M, Jurvelin JS. Ultrasound backscatter imaging provides frequency-dependent information on structure, composition and mechanical properties of human trabecular bone. Ultrasound Med Biol 2009; 35: 1376-1384.
144) Dogdas B, Shattuck DW, Leahy RM. Segmentation of skull and scalp in 3-D human MRI using mathematical morphology. Hum Brain Mapp 2005; 26: 273-285.
145) Snyder SM, Schneider E. Estimation of mechanical properties of cortical bone by computed tomography. J Orthop Res 1991; 9: 422-431.
146) Ciarelli M, Goldstein S, Kuhn J, Cody D, Brown M. Evaluation of orthogonal mechanical properties

and density of human trabecular bone from the major metaphyseal regions with materials testing and computed tomography. J Orthop Res 1991; 9: 674-682.
147) Van der Jeught S, Dirckx JJ, Aerts JR, Bradu A, Podoleanu AG, Buytaert JA. Full-field thickness distribution of human tympanic membrane obtained with optical coherence tomography. J Assoc Res Otolaryngol 2013; 14: 483-494.
148) Rude R, Gruber H, Wei L, Frausto A, Mills B. Magnesium deficiency: effect on bone and mineral metabolism in the mouse. Calcif Tissue Int 2003; 72: 32-41.
149) Heinrichs WL, Fong P, Flannery M, Heinrichs SC, Crooks LE, Spindle A, Pedersen RA. Midgestational exposure of pregnant BALBc mice to magnetic resonance imaging conditions. Magn Reson Imaging 1988; 6: 305-313.
150) Jämsä T, Jalovaara P, Peng Z, Väänänen HK, Tuukkanen J. Comparison of three-point bending test and peripheral quantitative computed tomography analysis in the evaluation of the strength of mouse femur and tibia. Bone 1998; 23: 155-161.
151) Pasquesi JJ, Schlachter SC, Boppart MD, Chaney E, Kaufman SJ, Boppart SA. In vivo detection of exercise-induced ultrastructural changes in genetically-altered murine skeletal muscle using polarization-sensitive optical coherence tomography. Opt Express 2006; 14: 1547-1556.
152) Kang BT, Park C, Yoo JH, Gu SH, Jang DP, Kim YB, Woo EJ, Kim DY, Cho ZH, Park HM. 18F-fluorodeoxyglucose positron emission tomography and magnetic resonance imaging findings of primary intracranial histiocytic sarcoma in a dog. J Vet Med Sci 2009; 71: 1397-1401.
153) Sant'Anna EF, Leven RM, Virdi AS, Sumner D. Effect of low intensity pulsed ultrasound and BMP-2 on rat bone marrow stromal cell gene expression. J Orthop Res 2005; 23: 646-652.
154) Jendelová P, Herynek V, Urdzikova L, Glogarová K, Kroupová J, Andersson B, Bryja V, Burian M, Hájek M, Syková E. Magnetic resonance tracking of transplanted bone marrow and embryonic stem cells labeled by iron oxide nanoparticles in rat brain and spinal cord. J Neurosci Res 2004; 76: 232-243.
155) Barou O, Valentin D, Vico L, Tirode C, Barbier A, Alexandre C, Lafage-Proust MH. High-resolution three-dimensional micro-computed tomography detects bone loss and changes in trabecular architecture early: comparison with DEXA and bone histomorphometry in a rat model of disuse osteoporosis. Invest Radiol 2002; 37: 40-46.
156) Patel NA, Zoeller J, Stamper DL, Fujimoto JG, Brezinski ME. Monitoring osteoarthritis in the rat model using optical coherence tomography. IEEE Trans Med Imaging 2005; 24: 155-159.
157) Pottier G, Bernards N, Dollé F, Boisgard R. [18F] DPA-714 as a biomarker for positron emission tomography imaging of rheumatoid arthritis in an animal model. Arthrit Res Ther 2014; 16: R69.
158) Enzmann DR, Britt RH, Lyons B, Buxton T, Wilson D. Experimental study of high-resolution ultrasound imaging of hemorrhage, bone fragments, and foreign bodies in head trauma. J Neurosurg 1981; 54: 304-309.
159) Lipsitz D, Levitski RE, Chauvet AE, Berry WL. Magnetic resonance imaging features of cervical stenotic myelopathy in 21 dogs. Vet Radiol Ultrasound 2001; 42: 20-27.
160) Davis GJ, Kapatkin AS, Craig LE, Heins GS, Wortman JA. Comparison of radiography, computed tomography, and magnetic resonance imaging for evaluation of appendicular osteosarcoma in dogs. J Am Vet Med Assoc 2002; 220: 1171-1176.
161) Park JY, Chung JH, Lee JS, Kim HJ, Choi SH, Jung UW. Comparisons of the diagnostic accuracies of optical coherence tomography, micro-computed tomography, and histology in periodontal disease: an ex vivo study. J Periodontal Implant Sci 2017; 47: 30-40.
162) Greenwood PL, Slepetis RM, McPhee MJ, Bell AW. Technical report: Prediction of stage of pregnancy in prolific sheep using ultrasound measurement of fetal bones. Reprod Fertil Dev 2002; 14: 7-13.
163) Nebelung S, Marx U, Brill N, Arbab D, Quack V, Jahr H, Tingart M, Zhou B, Stoffel M, Schmitt R, Rath B. Morphometric grading of osteoarthritis by optical coherence tomography--an ex vivo study. J Orthop Res 2014; 32: 1381-1388.
164) de Terlizzi F, Battista S, Cavani F, Canè V, Cadossi R. Influence of bone tissue density and elasticity on ultrasound propagation: an in vitro study. J Bone Miner Res 2000; 15: 2458-2466.
165) Mitchell A, Scholz A, Wang P, Song H. Body composition analysis of the pig by magnetic resonance imaging. J Anim Sci 2001; 79: 1800-1813.
166) Sun Z, Smith T, Kortam S, Kim D-G, Tee BC, Fields H. Effect of bone thickness on alveolar bone-height measurements from cone-beam computed tomography images. Am J Orthod Dentofacial Orthop 2011; 139: e117-e127.
167) Colston BW, Everett MJ, Da Silva LB, Otis LL, Stroeve P, Nathel H. Imaging of hard-and soft-tissue structure in the oral cavity by optical coherence tomography. Appl Opt 1998; 37: 3582-3585.
168) Beshara S, Lundqvist H, Sundin J, Lubberink M, Tolmachev V, Valind S, Antoni G, Långström B, Danielson BG. Kinetic analysis of 52Fe-labelled iron (III) hydroxide–sucrose complex following bolus administration using positron emission tomography. Br J Haematol 1999; 104: 288-295.
169) Lees S, Heeley JD, Cleary PF. A study of some properties of a sample of bovine cortical bone using ultrasound. Calcif Tissue Int 1979; 29: 107-117.
170) Majumdar S, Link TM, Augat P, Lin JC, Newitt D, Lane NE, Genant HK. Trabecular bone architecture in the distal radius using magnetic resonance imaging in subjects with fractures of the proximal femur. Osteoporos Int 1999; 10: 231-239.
171) Rodriguez A, Anastassov GE, Lee H, Buchbinder D, Wettan H. Maxillary sinus augmentation with deproteinated bovine bone and platelet rich plasma with simultaneous insertion of endosseous implants. J Oral Maxillofac Surg 2003; 61: 157-163.

172) Bykov A, Hautala T, Kinnunen M, Popov A, Karhula S, Saarakkala S, Nieminen MT, Tuchin V, Meglinski I. Imaging of subchondral bone by optical coherence tomography upon optical clearing of articular cartilage. J Biophotonics 2016; 9: 270-275.

173) Burger C, Goerres G, Schoenes S, Buck A, Lonn A, Von Schulthess G. PET attenuation coefficients from CT images: experimental evaluation of the transformation of CT into PET 511-keV attenuation coefficients. Eur J Nucl Med Mol Imaging 2002; 29: 922-927.